

7. SHALLOW SEISMIC STRUCTURE OF EASTERN PACIFIC OCEAN CRUST AT ODP SITE 1224¹

Y.F. Sun,² J. Kasahara,³ R. Stephen,⁴ G.T. Baechle,⁵ G.P. Eberli,⁵
H. Hoskins,⁴ M. Nakamura,³ and Y.C. Teng⁶

ABSTRACT

Ocean Drilling Program Site 1224 is located about halfway between California and Hawaii in the eastern Pacific and was drilled, cored, and logged during Leg 200. The upper oceanic crust (~45–50 Ma) at this site was previously considered to be simple and uniform. The core and logging data acquired at this site, however, reveal five distinct units differentiated by petrophysical property variations in the ~145-m-thick basement. In addition, a hydrothermal vein exists near the bottom of the basement that penetrates the drilled location. For the first time, this study provides seismic evidence of the five-layer structure of the upper oceanic crust around the site. Through advanced high-resolution seismic processing, the boundaries of these logging units can be clearly identified on the processed seismic section and extended laterally away from the drill hole. The fault systems around the site can also be imaged clearly. Relative to the seafloor reflection, the hydrothermal vein has a unique reversed polarity seismic signature. Seismic analysis also indicates that the hydrothermal vein remains open to nearby faults connected to the seafloor. This finding provides geophysical evidence of hydrothermal circulation in the upper oceanic crust that may host observed microbial activity at the site.

¹Sun, Y.F., Kasahara, J., Stephen, R., Baechle, G.T., Eberli, G.P., Hoskins, H., Nakamura, M., and Teng, Y.C., 2006. Shallow seismic structure of eastern Pacific Ocean crust at ODP Site 1224. In Kasahara, J., Stephen, R.A., Acton, G.D., and Frey, F.A. (Eds.), *Proc. ODP, Sci. Results*, 200, 1–22 [Online]. Available from World Wide Web: <http://www-odp.tamu.edu/publications/200_SR/VOLUME/CHAPTERS/006.PDF>. [Cited YYYY-MM-DD]

²Lamont-Doherty Earth Observatory of Columbia University, 61 Route 9W, Palisades NY 10964, USA.

sunyf@ldeo.columbia.edu

³Earthquake Research Institute, University of Tokyo, 1-1-1 Yayoi, Bunko-ku, Tokyo 113-0032, Japan.

⁴Department of Geology and Geophysics, Woods Hole Oceanographic Institution, MS 24, 360 Woods Hole Road, Woods Hole MA 02543-1524, USA.

⁵Comparative Sedimentology Laboratory, Rosenstiel School of Marine and Atmospheric Science, University of Miami, 4600 Rickenbacker Causeway, Miami FL 33149, USA.

⁶Femarco, Inc., New York NY 10025, USA.

INTRODUCTION

During Ocean Drilling Program Leg 200, 16 December 2001–27 January 2002, Hole 1224D (27°53.3699'N, 141°58.7525'W) was drilled in the eastern Pacific (Fig. F1A) for later downhole installation of a broadband seismometer as a part of the global Oceanic Seismic Network (Stephen, Kasahara, Acton, et al., 2003). Within 20 m of this seismometer hole, Hole 1224F (27°53.3634'N, 141°58.7567'W) was drilled to a total depth of 174.5 meters below seafloor (mbsf) for logging to characterize the physical and chemical properties of the basement at the site.

The oceanic crust at Site 1224 has an age of ~45–50 Ma with a spreading rate of ~140 mm/yr (full rate). Prior studies (e.g., Raitt, 1963; Menard, 1964) concluded that the upper oceanic crust on the Pacific plate with age <100 Ma exhibits no internal structure other than being simple and uniform. The core and logging data acquired at this site, however, revealed five distinct logging units differentiated by petrophysical property variations within the <150-m-thick upper basement (Stephen, Kasahara, Acton, et al., 2003). A hydrothermal vein was identified near the bottom of the drill hole from logging data analysis. Microbial activity and fungal fossils were also observed at this site (Stephen, Kasahara, Acton, et al., 2003). It is quite evident that the physical and structural properties of the upper oceanic crust at this site are more complicated than previously inferred using seismic technology in the 1960s.

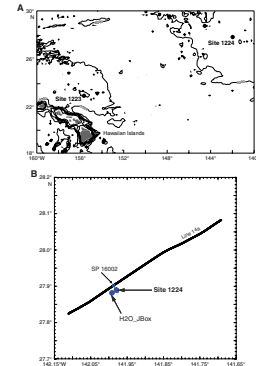
In this paper, we provide for the first time seismic evidence of the five-layer structure of the upper oceanic crust at the drilled site correlated with the logging units. Using advanced methods of seismic resolution enhancement, the boundaries of these logging units as well as the fault systems can be clearly imaged. The hydrothermal vein has a strong seismic signature with a negative polarity compared with the seafloor reflection. Seismic data further show that there are faults linking the hydrothermal vein to the seafloor. The detailed methodology of core-log-seismic integration is described in Sun (2000, 2004) and Sun and Goldberg (2000). Details of the seismic resolution enhancement method are given by Sun (2004).

CORE AND LOGGING DATA

The seismometer hole, Hole 1224D, was cored from 25.5 to 59 mbsf with 15.65 m of core recovered. Hole 1224F is <20 m southeast of Hole 1224D and was cored to a depth of 174.5 mbsf with 37.7 m of core recovered. Downhole logging measurements in Hole 1224F were made to a total depth (TD) of 174.5 mbsf. The water depth was 4967 m and the sediment thickness was ~28 m at the site. The base of the pipe in Hole 1224F was at 35 mbsf during logging.

Hole 1224F was logged using a nearly complete suite of wireline logging tools that measured nuclear, acoustic and shear, and electrical and magnetic properties. Borehole electrical image and temperature logs were also acquired. Because of the low core recovery (~20%), logging measurements in Hole 1224F were vital for inferring the structure of the upper oceanic crust at this site. Detailed descriptions of the logging tools and preliminary logging data analysis are referred to Stephen, Kasahara, Acton, et al. (2003).

F1. Location map, p. 10.



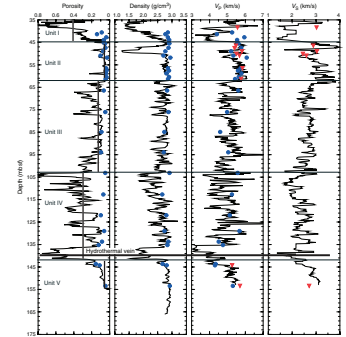
The density (RHOB), neutron porosity (NPHI), compressional wave velocity (V_p), and shear wave velocity (V_s) acquired using the logging tools and used in this seismic study are shown in Figure F2. The five logging units shown in Figure F2 were classified using these and other logging data and based on core descriptions and downhole Formation MicroScanner (FMS) image analysis (Stephen, Kasahara, Acton, et al. 2003). Unit I (above 45 mbsf) contains high-porosity, low-density, and low-velocity rocks filled with basaltic fragments. Unit II (45–63 mbsf) is characterized by uniformly high velocity and low porosity massive basalt flows. Unit III (63–103 mbsf) consists of relatively uniform and high-velocity breccia and sheeted lava flows. Unit IV (103–142 mbsf) contains pillow lavas as seen from the FMS log. Unit V (below 142 mbsf) is composed of dense basalts with a uniform density of ~ 2.9 g/cm³. In addition, a hydrothermal vein between 138 and 142 mbsf was detected by all the logging tools, particularly by elevated temperature and natural gamma radiation (Stephen, Kasahara, Acton, et al. 2003).

Shipboard moisture and density and compressional wave velocity measurements were compared with in situ downhole logging data. Descriptions of these shipboard measurements are referred to Stephen, Kasahara, Acton, et al. (2003). As shown in Figure F2, core measurements of porosity, density, and compressional wave velocity agree well with in situ downhole logging data where the rocks are dense, especially in Unit II. In other units, filled with breccia and pillows, core measurements approximate only the limits of the dense rock matrixes without sensing any existence of large-scale structures. Shore-based compressional and shear wave velocity measurements under elevated pressures were obtained on 11 samples without visible fractures from both Holes 1224D and 1224F. Good ultrasonic shear wave signals were obtained only on 7 samples. The compressional and shear wave velocity measurements at estimated in situ pressure are plotted in Figure F2 as triangles. In the dense Unit II, both shipboard and shore-based wave velocity measurements agree well with downhole logging data. Figure F3 shows typical velocity measurement results under pressure for a seawater-saturated core plug from Section 200-1224D-2R-3 from a depth of ~ 38 mbsf. The pressure effect on wave velocity under saturated condition is minimal for dense basaltic rocks, as expected, and the shear wave anisotropy is negligible.

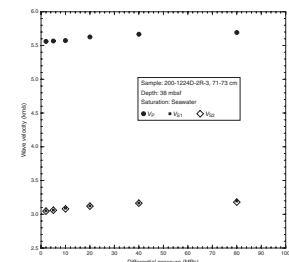
SEISMIC DATA AND ANALYSIS

A survey of the Hawaii-2 cable between 140° and 143°W was carried out in August 1997 on the *Revelle* (Stephen et al., 1997), during which single-channel seismic (SCS) data were acquired along the cable track starting at 140°W and heading southwest. Site 1224 is to the southwest of a well-surveyed block but is bracketed by two parallel SCS lines (Line 14a in Figure F1B and a second SCS line not shown in the figure). The seismic source from the generator injector (GI) gun from Seismic Systems, Inc. was run in “pure GI mode.” The generator chamber is 45 in³, and the injector chamber is 105 in³. It was estimated that the GI gun was towed at a depth of 8 m or less (Stephen et al., 1997). The streamer consists of two active sections towed at a depth of <20 m. The digital data were acquired on an analog-to-digital acquisition system from the School of Ocean and Earth Science and Technology (SOEST) (Hawaii, USA) (Stephen et al., 1997) and were recorded with a sampling interval of 1 ms and a time delay of 5 s. The spacing between shots was 40 m. A

F2. Physical properties, Hole 1224F, p. 11.



F3. Wave velocity vs. differential pressure, Hole 1224D, p. 12.



portion of the seismic section along Line 14a (the North line) shown in Figure F4 consists of 200 shotpoints (SPs) around SP 16002. SP 16002 is the closest point of approach to Site 1224.

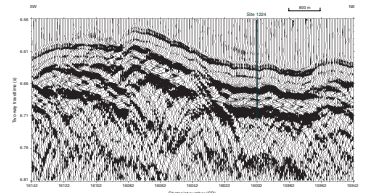
The amplitude spectrum of the original seismic data recorded at SP 16002 is shown in Figure F5A. The amplitude spectrum of recorded seismic data depends on the source signal, hydrophone response, survey design specifications, Earth structures that the seismic signal passes through, and environmental noise. The GI gun outputs a single large spike with essentially no bubble pulse. The width of the single large spike on the blast phone at the gun was measured to be ~10 ms. Because of the source and receiver depth in the water and the existence of the air/water surface (“ghost effect”), the resultant wavelet recorded is a composite waveform of a three-peaked pulse with a central negative peak twice as large in amplitude as the positive first and third pulses. This situation is common to nearly all marine seismic surveys. The resultant wavelet of the Hawaii-2 observatory (H2O) seismic site survey was thus estimated to have a dominant frequency of 33 Hz (Stephen et al., 1997). The original spectrum for SP 16002 in Figure F5A indeed shows strong seismic energy distributed in the frequency components between 10 and 50 Hz. Moreover, the spectrum also reveals that there are two more energy bands in the original seismic signal with dominant frequencies of 70 and 160 Hz, respectively. These two higher-frequency energy bands shown in Figure F5 for SP 16002 are typical for the recorded seismic data of the survey, and they are seismic signals rather than environmental noise. The three-banded amplitude spectrum of the original record shown in Figure F5 agrees very well with those typically recorded with an air gun at a depth of 10 m and the streamer at a depth of 15 m (Evans, 1997, p. 154). The direct current component due to the ghost effect is also evident in the original spectrum.

Downhole logging data indicate that within the 140-m basement drilled at Site 1224 there are layered structures on the log scale. Synthetic seismograms with different wavelets of variable dominant frequencies could help determine in what seismic frequency bands such layered structures can be identified. The process of synthetic seismogram generation is illustrated in Figures F6 and F7. Using downhole density and compressional wave velocity data, an impedance profile, which is a product of density and velocity ($Z = \rho \times V$), is obtained, as shown vs. depth in Figure F6 and vs. two-way traveltime in Figure F7. The density and wave velocity of seawater is assumed to be 1.024 g/cm³ and 1.5 km/s, respectively. An average density and velocity for the 28-m sediment section of 1.52 g/cm³ and 1.5 km/s, respectively, is estimated from shipboard core measurements. The density and velocity for the basement rock between 28 and 35 mbsf are assumed to be a single-value extrapolation of the logging data at 35 mbsf. A reflection coefficient (RC) series can then be calculated using the formula

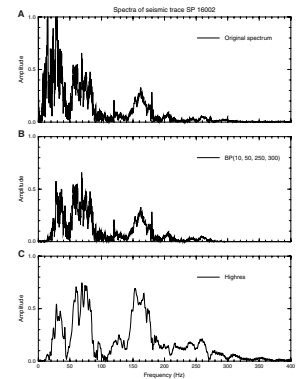
$$r_i = (Z_{i+1} - Z_i) / (Z_i + Z_{i+1}),$$

from the impedance at a logging depth sample i and the impedance at the adjacent logging depth sample $i + 1$. The calculated RC series is termed as primary RC without considering multiple reflections, which are shown in depth in Figure F6 and in time in Figure F7. A synthetic seismogram is usually generated using the RC series convolved with a source wavelet. To demonstrate the convolution process, a Ricker wavelet with a dominant frequency of 75 Hz, labeled as Ricker (75Hz) in Fig-

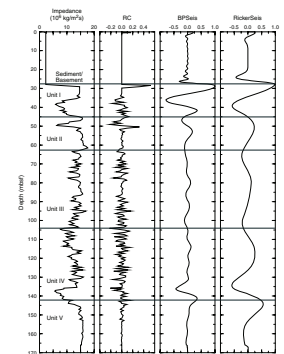
F4. Unprocessed SCS Line 14a, p. 13.



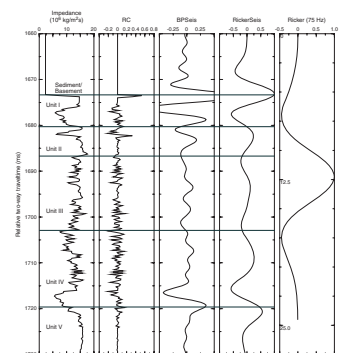
F5. Seismic trace spectra, p. 14.



F6. Synthetic seismogram vs. depth, p. 15.



F7. Synthetic seismogram vs. TWT, p. 16.

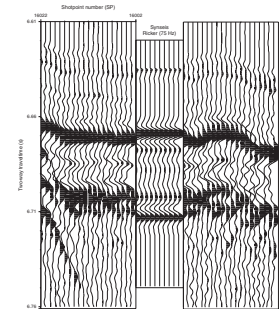


ure F7, is used to calculate the seismogram, shown as RickerSeis in depth in Figure F6 and time in Figure F7. By reversing its polarity, the Ricker wavelet is the ideal presentation of the composite air gun-hydrophone signature. A dominant frequency of 75 Hz is used instead of 33 Hz, as indicated from the seismic data, to show possible effects of structures on the synthetic seismogram. From the synthetic seismogram (RickerSeis) shown in Figures F6 and F7 and its comparison with unprocessed SCS data at Site 1224 in Figure F8, the traveltime for reflections from the water/sediment and sediment/basement interfaces agrees well with the field SCS data. However, the seismic energy in the 10- to 50-Hz frequency band in both the synthetic seismogram and field SCS data masks the detailed basement structures revealed by the downhole logs.

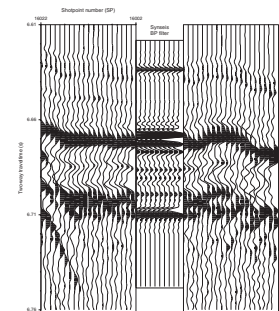
It is evident that the resolution of the SCS data needs to be increased with proper seismic data processing algorithms. One simple way is to apply a bandpass (BP) filter to the seismic data in order to eliminate the seismic energy in the frequency band of 10–50 Hz. By analyzing the original spectrum of the SCS data in Figure F5A, we use a bandpass filter of BP (10, 50, 250, 300) to keep all the seismic energy in the frequency band of 50–250 Hz as shown in Figure F5B. We apply the same bandpass filter to the RC series to retain only the structural information in the frequency band of 50–250 Hz so that the filtered RC series is effectively a synthetic seismogram that can be compared with filtered seismic data. The BP-filtered RC series is shown as BPSeis vs. depth in Figure F6 and vs. two-way traveltime in Figure F7. It is enlarged in Figure F7 to show detailed variations. The boundaries between sediment/basement interfaces and between different basement units are shown in two-way travel time in Figure F7. These boundaries are identified by comparison of the impedance and RC signatures on the time profile (Fig. F7) with the depth profile (Fig. F6). Figure F9 shows a comparison between the BP-filtered RC synthetic seismogram and unprocessed SCS data. A portion of BP-filtered SCS data is shown in Figure F10 in comparison with the BP-filtered RC synthetic seismogram. The amplitude spectrum of the BP-filtered SCS data recorded at SP 16002 is displayed in Figure F5B. The agreement between the synthetic seismogram and seismic data in Figure F10 is better than that shown in Figure F9 for the unfiltered SCS data.

In order to better reveal the shallow seismic structure around Site 1224, the advanced high-resolution enhancement technique (Highres) was also used to improve the seismic signal/noise ratio and seismic resolution of the SCS data. Details of the Highres method are given by Sun (2004) in the attempt to resolve 0.5-m dolomite layers in modern marine sediments near the Japan Trench. The amplitude spectrum of the Highres-processed seismic trace at SP 16002 is shown in Figure F5C. In comparison with the amplitude spectrum after simple BP filtering shown in Figure F5B, it shows that Highres enhances the seismic energy in the higher-frequency components within the valid seismic energy band, especially the energy centered at 160 Hz. Comparison of the Highres SCS data with the BP-filtered RC synthetic seismogram in Figure F11 demonstrates that both the seismic resolution and seismic quality are much improved relative to the simple filtered SCS data. The basement units are identified following the seismic signatures of the BP-filtered RC synthetic seismogram in Figures F6 and F7 as will be explained later. Better seismic imaging and higher quality are also evident on the BP-filtered SCS data shown in Figure F12 in comparison with the unprocessed seismic section shown in Figure F4. This helps to demon-

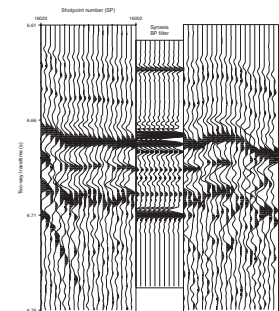
F8. Comparison of SCS data with Ricker wavelet, p. 17.



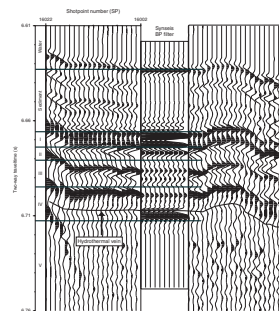
F9. Comparison of SCS data with BP filter, p. 18.



F10. Comparison of BP-filtered SCS data, p. 19.



F11. Comparison of SCS data with Highres enhancement, p. 20.



strate that even a simple filtering could improve seismic resolution to resolve the detailed crustal structures (Sun and Goldberg, 2000).

SEISMIC INTERPRETATION

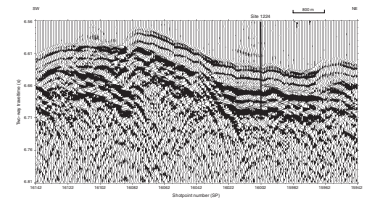
It is evident, as shown in Figures F6, F7, F8, and F9, that conventional seismic data with dominant frequency <100 Hz could hardly discern the detailed internal structure of the upper oceanic crust of <140 m thick revealed by logging and core data. In comparison with the original seismic section in Figure F4 and the BP-filtered seismic section in Figure F12, the quality of seismic data was drastically improved after Highres processing and resolution enhancement as shown in Figure F13. Many features, including clear-cut faults, can now be interpreted.

The seismic reflections from the boundaries of the five logging units can be easily identified on the Highres-processed SCS data as shown in Figure F11, in comparison with the synthetic seismogram generated at the drill site. Because SP 16002 is in the close vicinity of the drill site and the logging data are overall of good quality, the correlation between the synthetic seismogram and the Highres SCS data is quite good. Once the seafloor reflection or the water/sediment interface reflection in the Highres seismic section is tied up with that on the synthetic seismogram, the rest of the boundary reflections from the interface between the sediment and Unit I and those between the boundaries of the five logging units are well-aligned, as indicated in Figure F11.

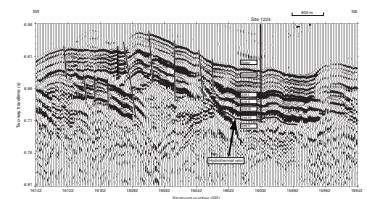
The reflections from the hydrothermal vein on both synthetic seismogram and Highres SCS data show reversed polarity compared to the seafloor reflection as shown in Figure F11. This is because of the low acoustic impedance contrast between the fluid-flowing hydrothermal vein and the adjacent basement interfaces as shown in Figure F6 and F7. Also in Figure F11, the reflection caused by the hydrothermal vein on the synthetic seismogram appears much stronger than that revealed on the Highres SCS data as well as the reflection from the interface between the sediment and basement Unit I. These are attributed to wash-out during drilling (Stephen, Kasahara, Acton, et al., 2003). Compared to the large impedance contrast caused by the presence of the hydrothermal vein, the impedance contrast, as well as the reflection and seismic amplitude of the boundary between Units IV and V, is relatively weak (Fig. F7). The boundary reflection between Units IV and V is thus masked by the presence of the nearby hydrothermal vein as shown in Figure F11; however it can still be clearly seen on the Highres SCS data as indicated in Figure F13.

Seismic imaging of the fault systems in the vicinity of Site 1224 was drastically improved as can be seen by a comparison of the unprocessed SCS section in Figure F4 and the Highres-processed SCS section in Figure F13. A fault cutting the structures at SP 16087 that is hardly visible in Figure F4 is clearly seen on the Highres SCS section in Figure F13. Many faults clearly imaged on the Highres seismic section could have been overlooked using the unprocessed data as shown in Figure F4. More importantly, the Highres seismic data in Figure F13 indicate that the hydrothermal vein identified using both logging and seismic data above the boundary between Units IV and V is connected to the fault cutting the sediment and basement structures at SP 16040. It is evident that this hydrothermal vein remains open to seawater through its link to the fault systems in the southwestward uplift. This finding could

F12. SCS after BP filtering, p. 21.



F13. SCS after Highres processing, p. 22.



provide geophysical evidence of possible hydrothermal circulation in this thin upper oceanic crust that may host the observed microbial activity at the drill site (Stephen, Kasahara, Acton, et al., 2003).

CONCLUSION

Prior knowledge assumes a homogeneous and uniform basement at Site 1224 that is typical of <100 Ma oceanic crust on the Pacific plate. The core and logging data, however, revealed five distinct units with varying petrophysical properties. Unit I (above 45 mbsf) contains high-porosity, low-density, and low-velocity rocks filled with basaltic fragments. Unit II (45–63 mbsf) is characterized by uniformly high velocity and low porosity massive basalt flows. Unit III (63–103mbsf) consists of relatively uniform and high-velocity breccia and sheeted lava flows. Unit IV (103–142 mbsf) contains pillow lavas as seen from the FMS log, and Unit V (below 142 mbsf) is composed of dense basalts with a uniform density of ~ 2.9 g/cm³. In addition, there is a hydrothermal vein at the base of the upper basement at the site based on FMS image analysis and interpretation of temperature and gamma ray logs.

This study further shows the seismic evidence of this five-layer structure of the upper oceanic crust in the vicinity of the drilled site. Conventional seismic data with dominant frequency <100 Hz cannot resolve the detailed internal structure of the <140-m-thick upper oceanic crust as revealed by logging and core data. Only through advanced seismic resolution enhancement can the boundaries of these logging units be clearly identified on the processed seismic section and extended laterally away from the drill hole. The fault systems at and near the site can also be imaged clearly. The hydrothermal vein can be uniquely identified by a strong reversed polarity seismic signature compared to the seafloor reflection. The hydrothermal vein is open to seawater through its link to the fault systems in the southwestward uplift. This finding may indicate geophysical evidence of possible hydrothermal circulation in the upper oceanic crust, which could help explain the observed microbial activity at the drill site.

During the course of this study, laboratory core measurements of porosity, density, compressional wave velocity, and shear wave velocity under pressure were also performed. These measurements agree well with in situ downhole logging data where the rocks are dense. In rocks filled with breccia and pillows, core measurements approximate only the limits of the dense rock matrixes, neglecting any existence of large-scale structures. This is the ever-challenging upscaling problem from the centimeter scale of the core plug to the meter scale of the logging measurements. It is evident that in situ downhole logging and high-resolution seismic data are essential to reveal meter-scale shallow oceanic crustal structures. This can become important and essential as the need increases to better map the internal structures of the upper oceanic crust and therefore understand the hydrothermal circulation systems and their associated microbial communities.

ACKNOWLEDGMENTS

This research used samples and/or data supplied by the Ocean Drilling Program (ODP). ODP is supported by the U.S. National Science Foundation (NSF) and participating countries under management of

Joint Oceanographic Institutions (JOI), Inc. The technical support from Leg 200 crew, staff, and scientists aboard the *JOIDES Resolution* is acknowledged. This research was supported by a U.S. National Science Foundation JOI/U.S. Science Advisory Committee grant. We thank the anonymous reviewers for their comments. We also thank Gary Acton for his helpful review.

REFERENCES

- Evans, B.J., 1997. *A Handbook for Seismic Data Acquisition in Exploration*: Tulsa (Society of Exploration Geophysicists).
- Menard, H.W., 1964. *Marine Geology of the Pacific*: New York (McGraw-Hill).
- Raitt, R.W., 1963. The crustal rocks. In Hill, M.N. (Ed.), *The Sea—Ideas and Observations on Progress in the Study of the Seas* (Vol. 3): *The Earth Beneath the Sea*: New York (Wiley-Interscience), 85–102.
- Stephen, R.A., Swift, S.A., and Greaves, R.J., 1997. *Bathymetry and Sediment Thickness Survey of the Hawaii-2 Cable*, WHOI-03-97: Woods Hole, MA (Woods Hole Oceanographic Institution).
- Stephen, R.A., Kasahara, J., Acton, G.D., et al., 2003. *Proc. ODP, Init. Repts.*, 200 [CD-ROM]. Available from: Ocean Drilling Program, Texas A&M University, College Station TX 77845-9547, USA. [[HTML](#)]
- Sun, Y.-F., 2000. Core-log-seismic integration in hemipelagic marine sediments on the eastern flank of the Juan de Fuca Ridge. In Fisher, A., Davis, E.E., and Escutia, C. (Eds.), *Proc. ODP, Sci. Results*, 168: College Station, TX (Ocean Drilling Program), 21–35. [[HTML](#)]
- Sun, Y.-F., 2004. Modeling seismic reflections from thin-bed dolomite layers in diatomite formation. *Isl. Arc*, 13:227–241.
- Sun, Y.F., and Goldberg, D., 2000. Characterization of the upper oceanic crust using high-resolution seismic amplitude modeling. In Dilek, Y., Moores, E., Elthon, D., and Nicolas, A. (Eds.), *Ophiolites and Oceanic Crust: New Insights from Field Studies and the Ocean Drilling Program*. Spec. Pap.—Geol. Soc. Am., 349:203–210.

Figure F1. Location map of (A) Site 1224 and (B) seismic Line 14a used in this study. Shotpoint (SP) 16002 is the closest point of approach to Site 1224. H2O_Jbox is the location of the Hawaii-2 Observatory junction box for downhole seismometer installation.

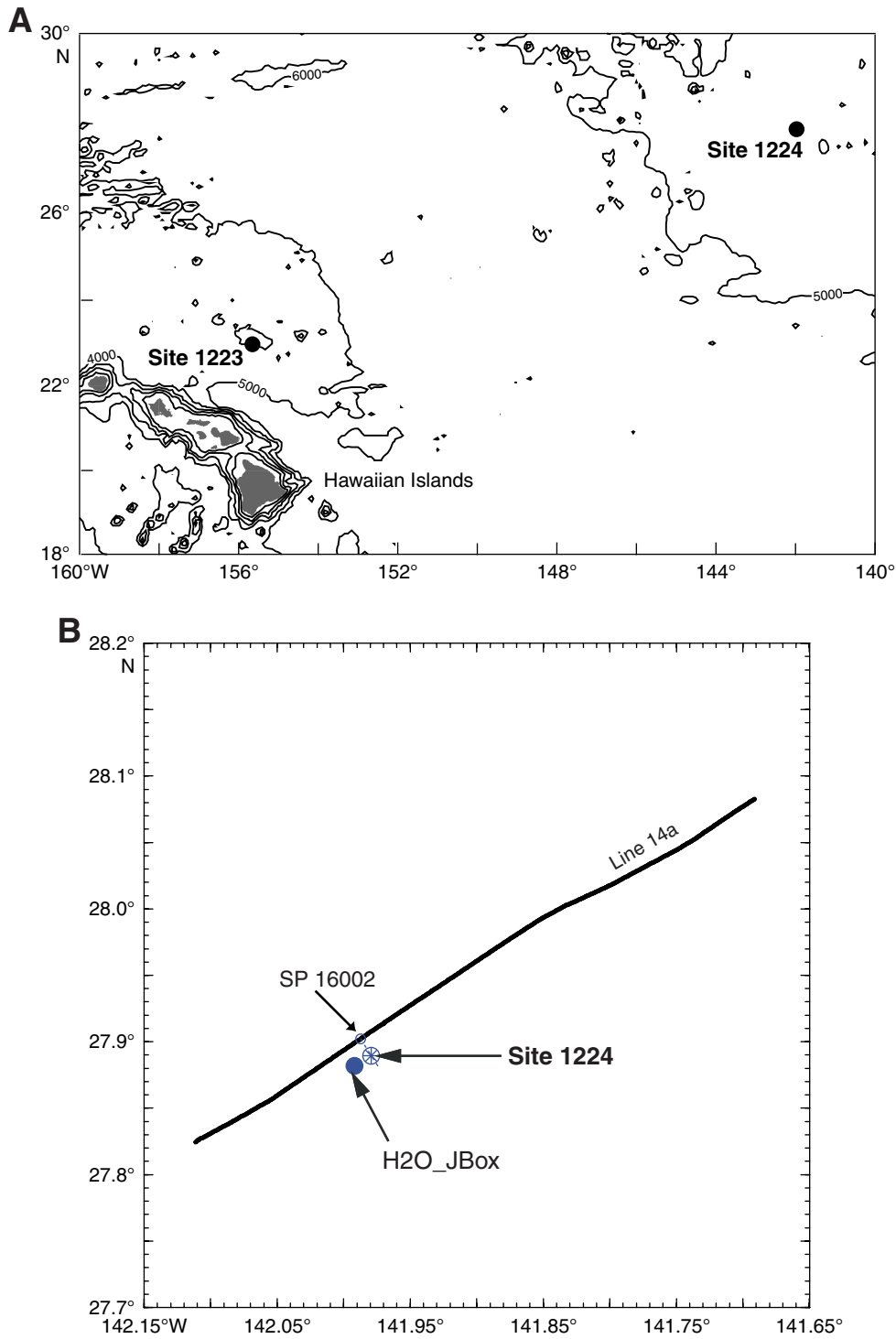


Figure F2. Downhole neutron porosity, density, compressional wave velocity (V_p), and shear wave velocity (V_s) obtained from Hole 1224F compared with shipboard core measurements (circles) and sonic measurements under pressure (triangles). The five logging units and the location of the hydrothermal vein are also shown.

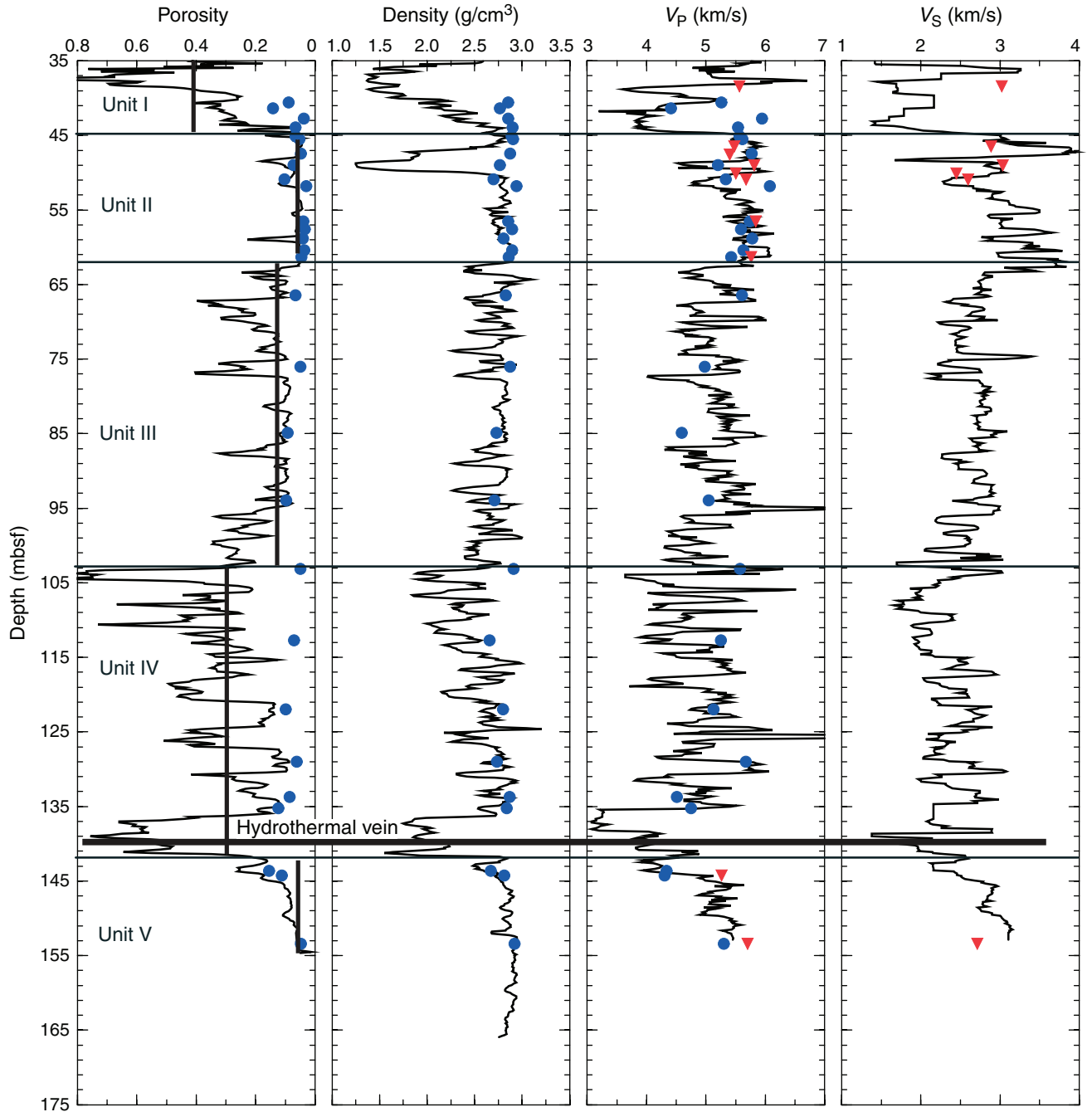


Figure F3. Ultrasonic wave velocity vs. differential pressure for seawater-saturated basaltic sample from 38 mbsf in seismometer Hole 1224D. The shear wave velocity measurements in two orthogonal directions (V_{S1} and V_{S2}) are nearly identical, showing no shear wave anisotropy at this depth.

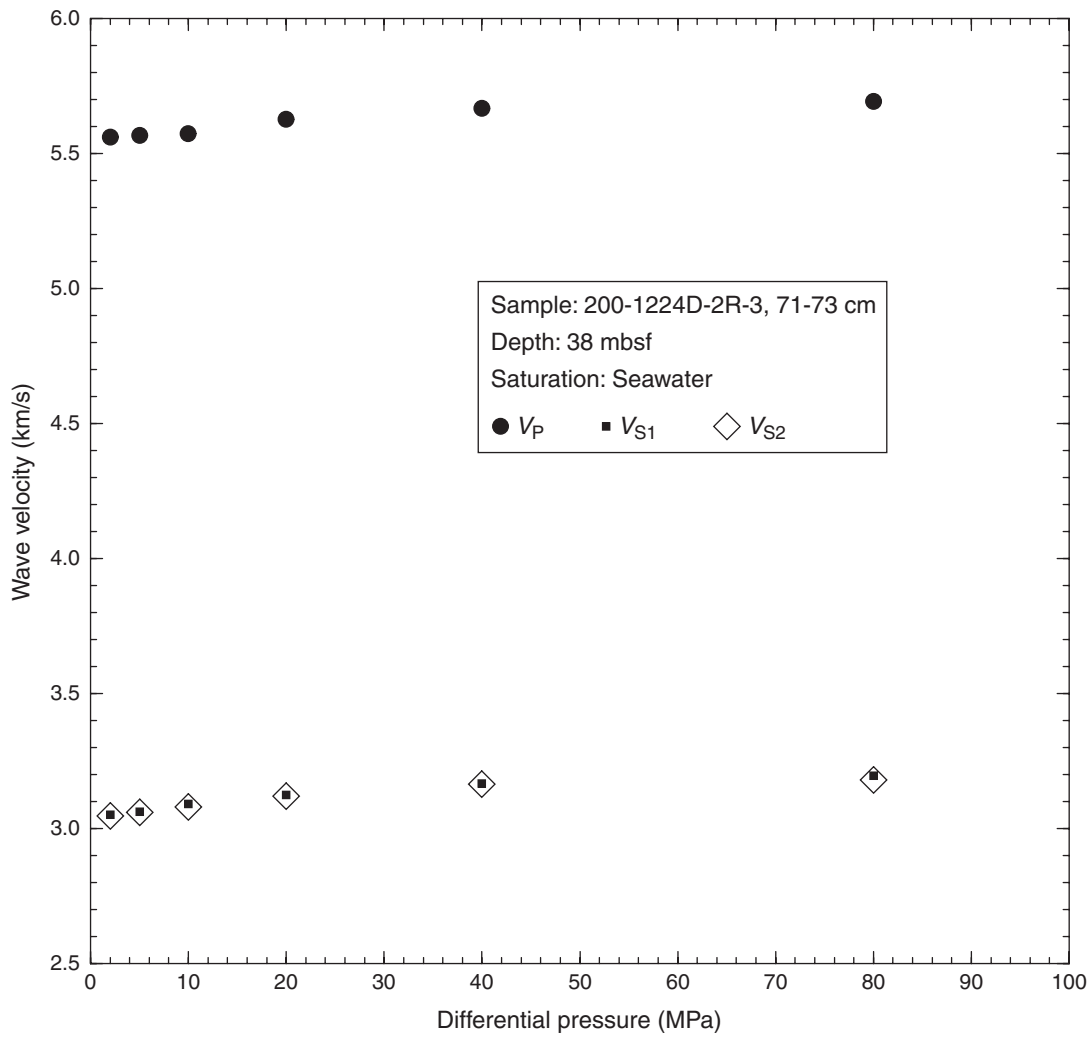


Figure F4. A portion of the unprocessed SCS Line 14a near Site 1224. Shotpoint (SP) 16002 is the closest point of approach to the site.

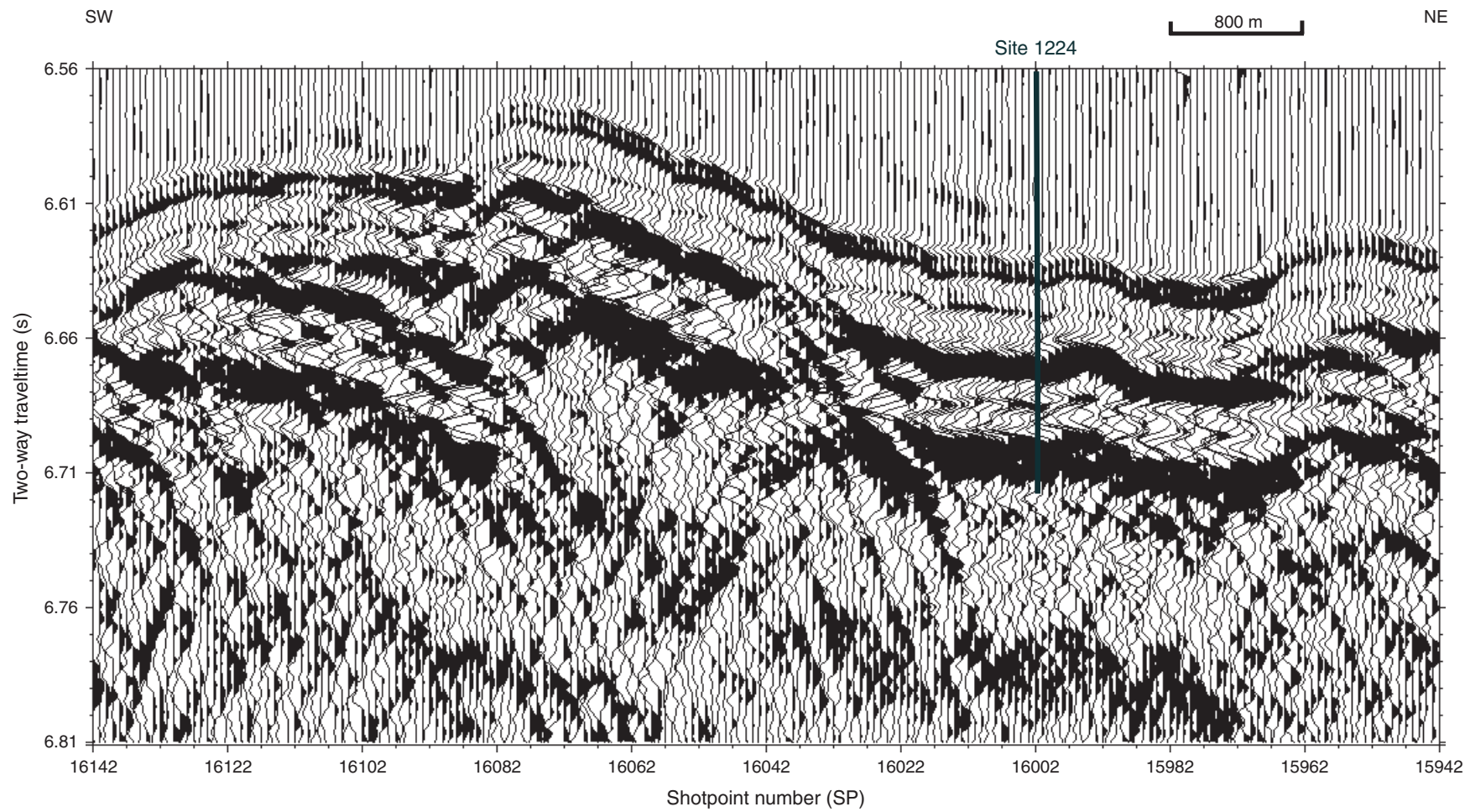


Figure F5. Spectra of seismic trace at shotpoint (SP) 16002 (A) before data processing, (B) after bandpass (BP) filtering, and (C) after high-resolution (Highres) enhancement.

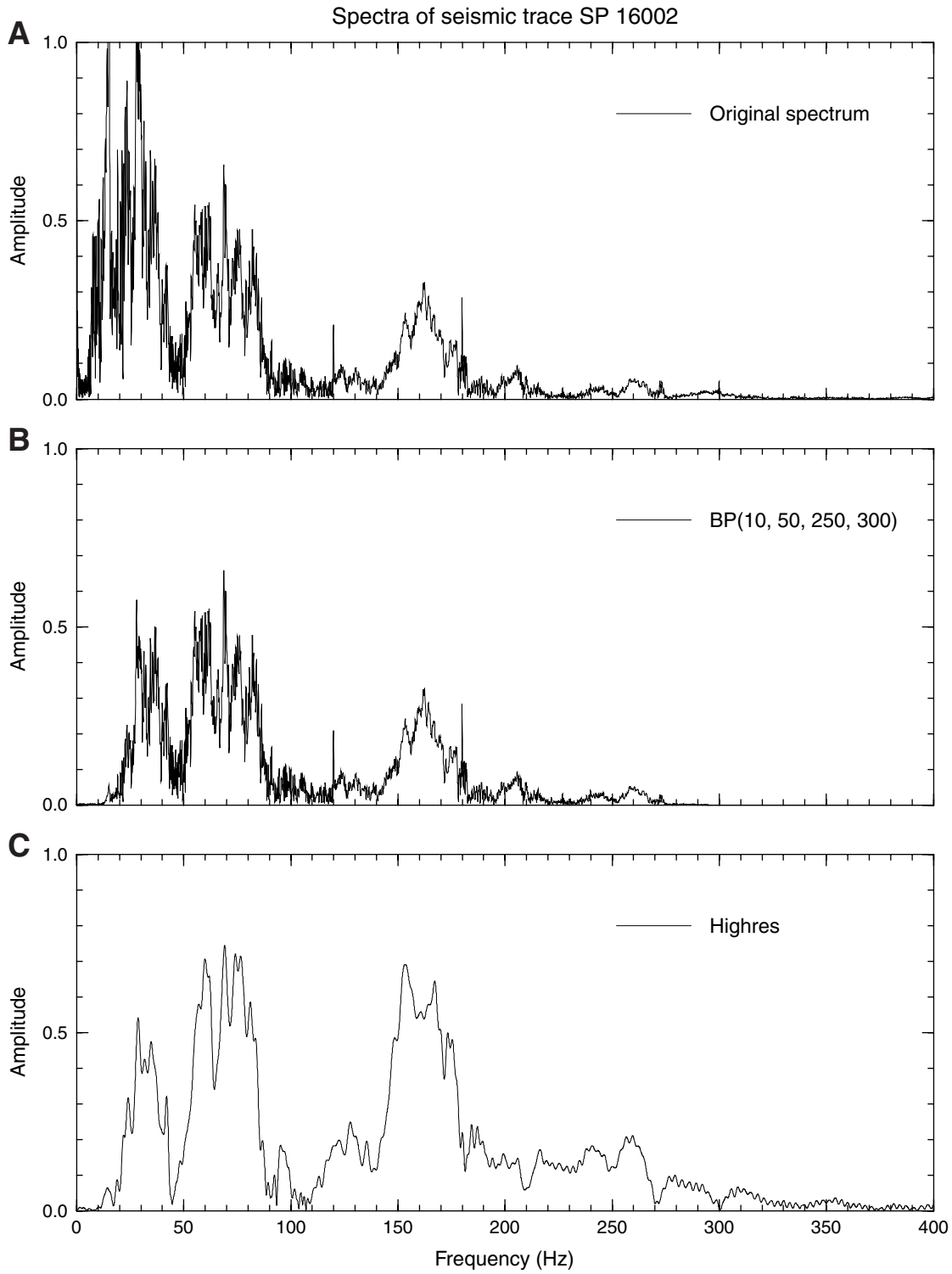


Figure F6. Synthetic seismogram at Hawaii-2 Observatory site vs. depth. Acoustic impedance and reflection coefficient (RC) series calculated from downhole density and compressional wave velocity logs in Hole 1224F. BPSeis = RC series after bandpass (BP) filter BP(10, 50, 250, 300) applied to RC data. RickerSeis = synthetic seismogram with RC series convolved with a Ricker wavelet with dominant frequency of 75 Hz (see Fig. F7).

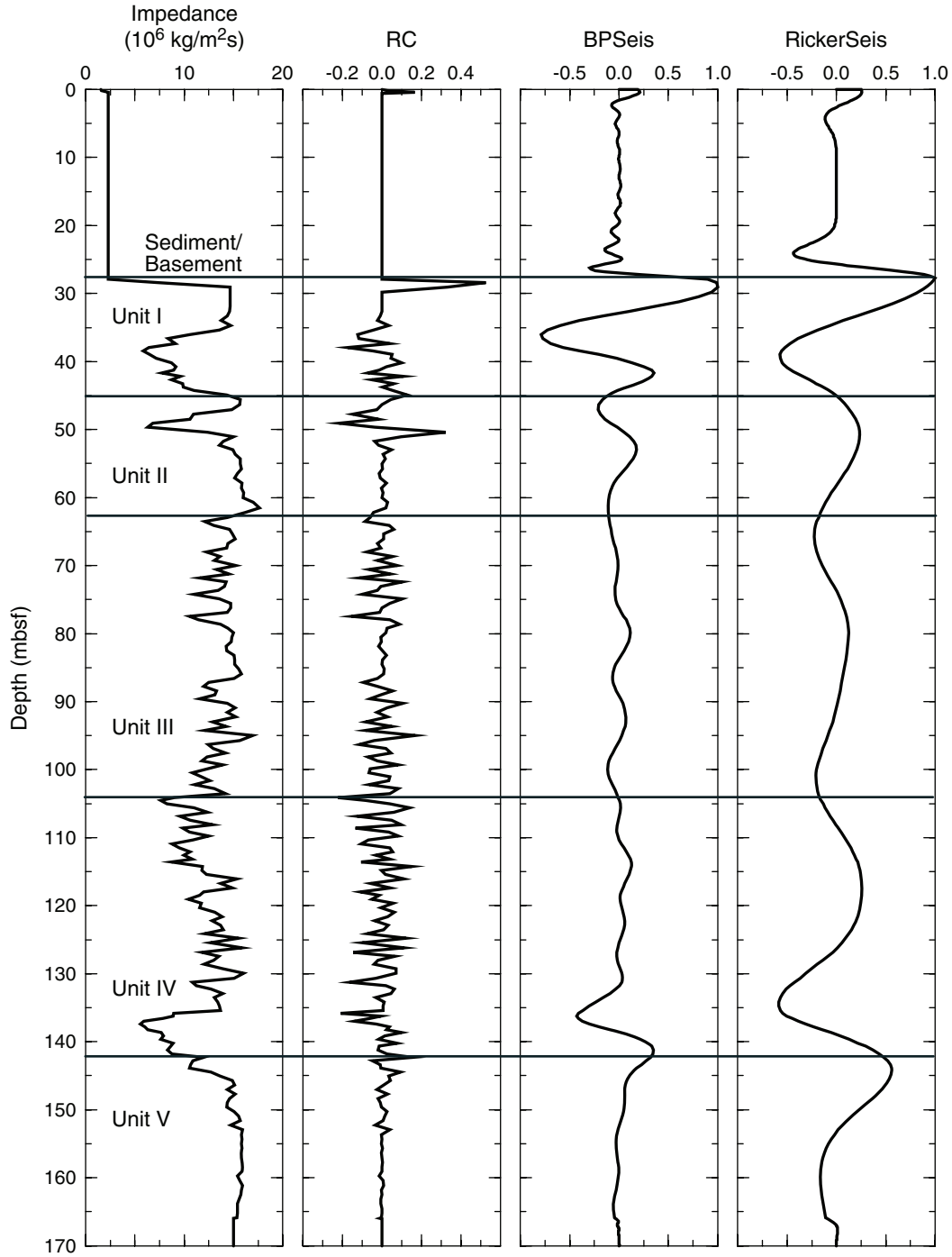


Figure F7. Synthetic seismogram at Hawaii-2 Observatory site vs. relative two-way traveltime. Acoustic impedance and reflection coefficient (RC) series calculated from downhole density and compressional wave velocity logs in Hole 1224F. BPSeis = RC series after bandpass (BP) filter BP(10, 50, 250, 300) applied to RC data. RickerSeis = synthetic seismogram with RC series convolved with a Ricker wavelet with dominant frequency of 75 Hz as shown by Ricker (75hz).

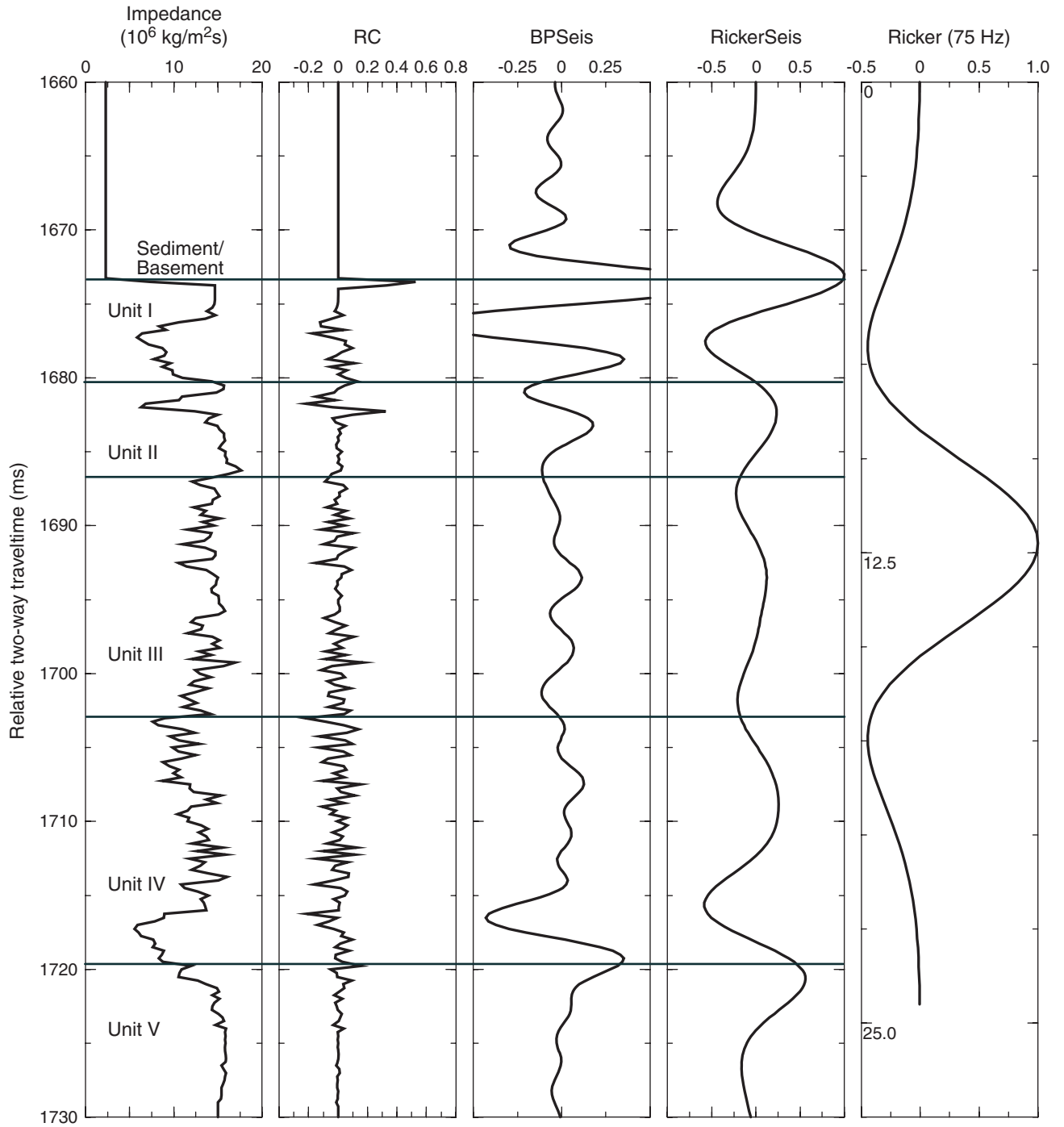


Figure F8. Comparison of unprocessed SCS data with the synthetic seismogram calculated using a Ricker wavelet of a dominant frequency of 75 Hz at shotpoint (SP) 16002. SP 16002 is the closest point of approach to Site 1224.

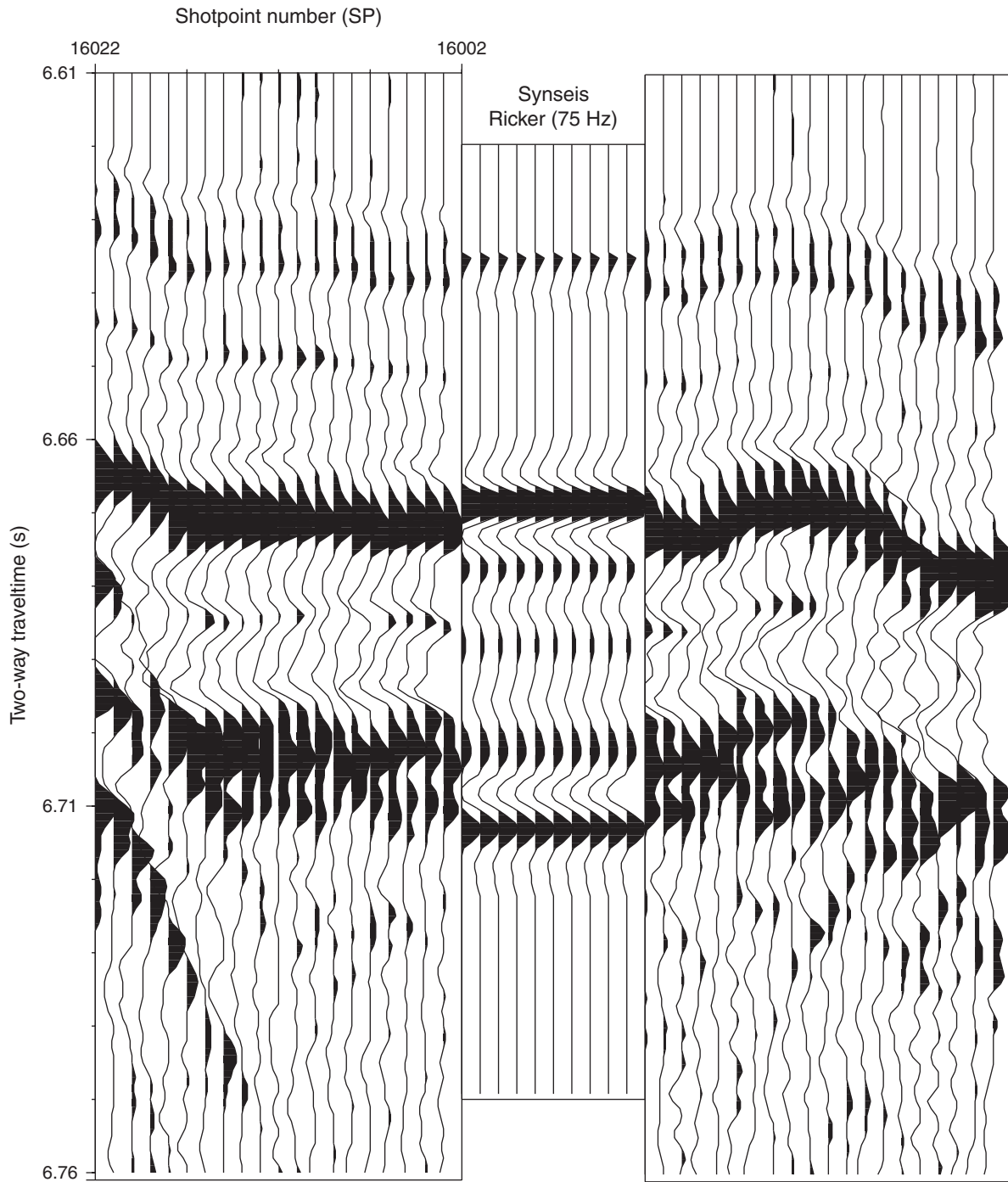


Figure F9. Comparison of unprocessed SCS data with the synthetic seismogram calculated by directly applying bandpass (BP) filter BP(10, 50, 250, 300) to the reflection coefficient series at shotpoint (SP) 16002. SP 16002 is the closest point of approach to Site 1224.

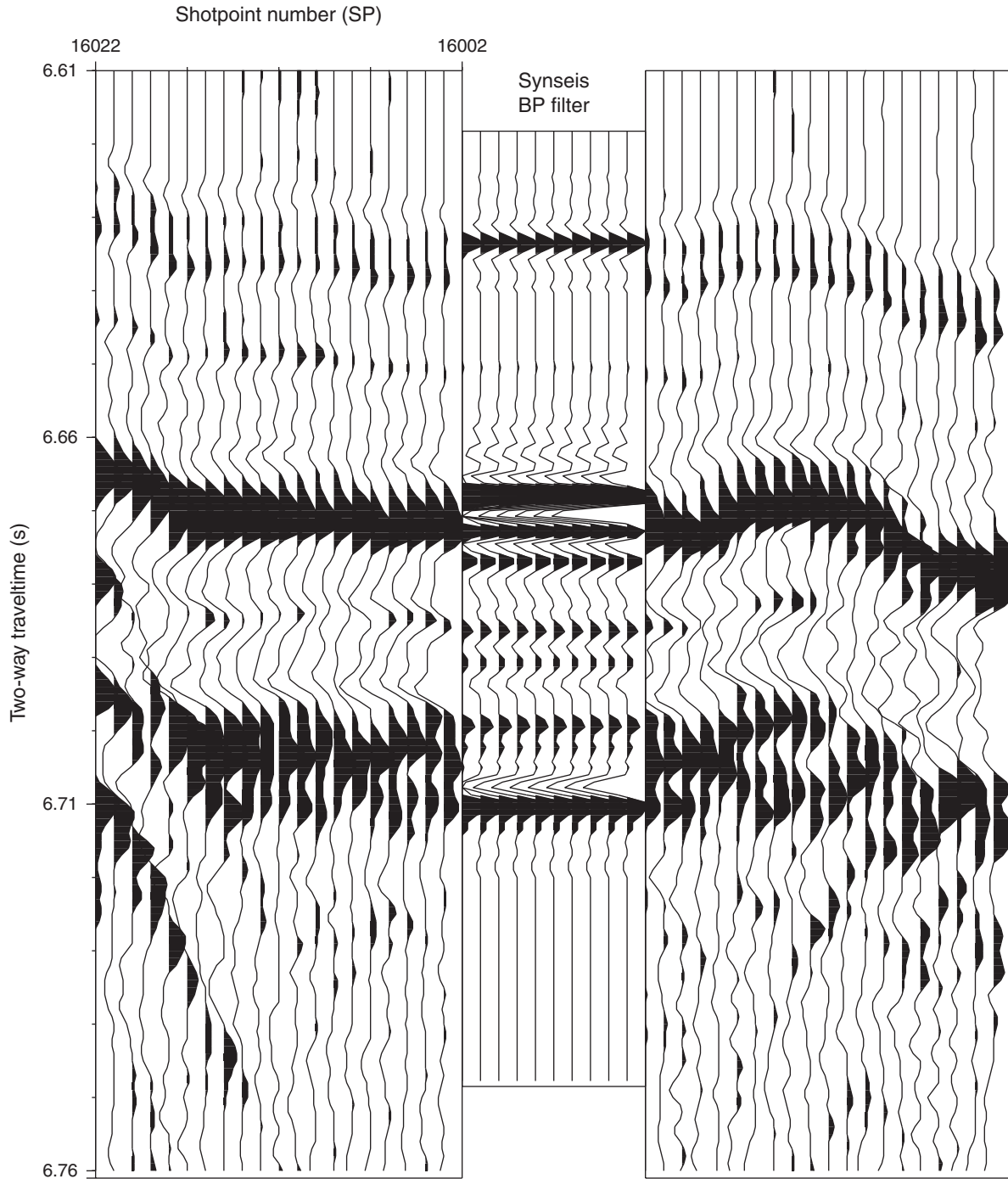


Figure F10. Comparison of bandpass (BP) filtered SCS data with the synthetic seismogram obtained by directly applying bandpass (BP) filter BP(10, 50, 250, 300) to both the SCS data and the reflection coefficient series at shotpoint (SP) 16002. Shotpoint SP 16002 is the closest point of approach to Site 1224.

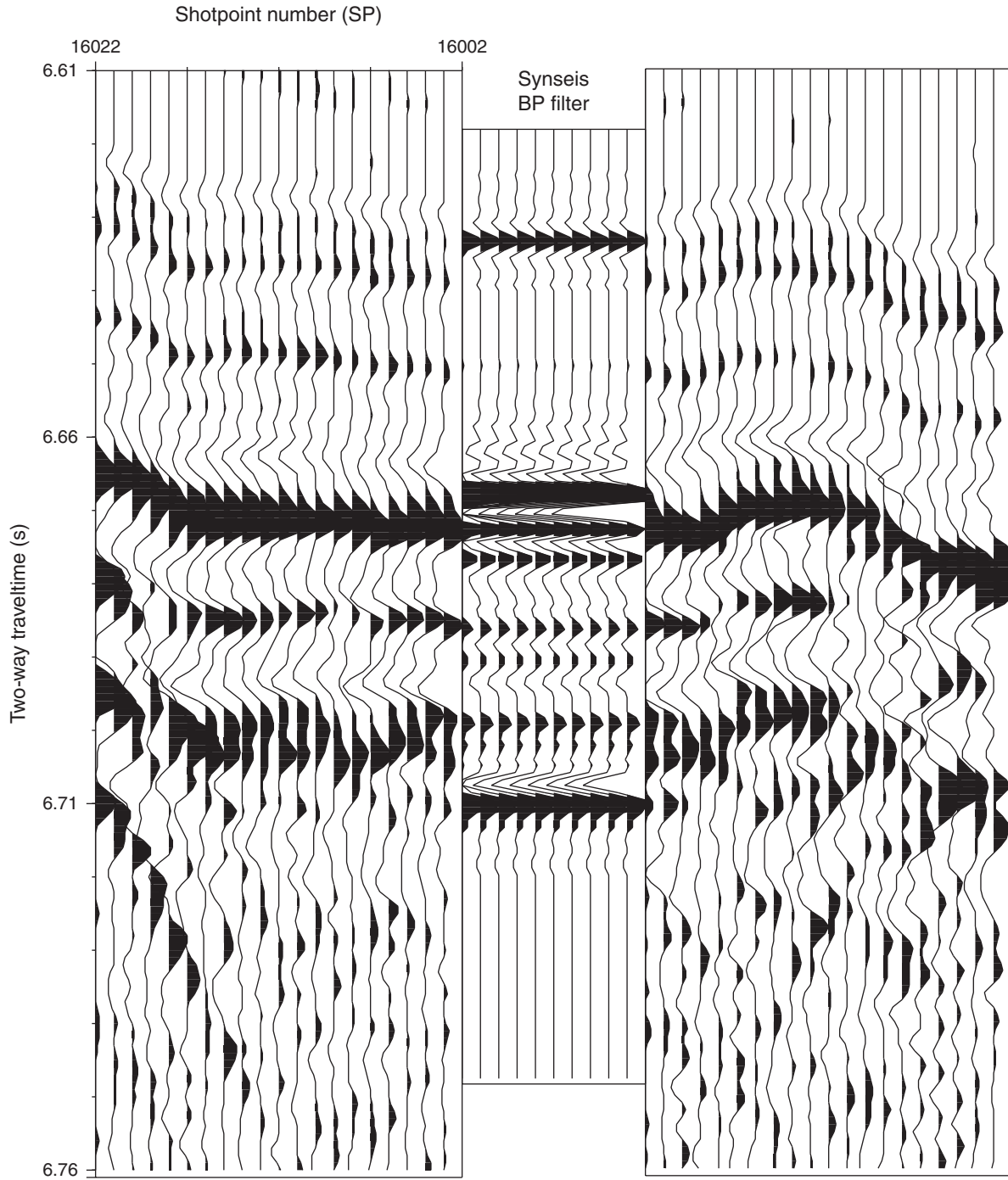


Figure F11. Comparison of the SCS data after high-resolution enhancement with the synthetic seismogram obtained by directly applying bandpass (BP) filter BP(10, 50, 250, 300) to the reflection coefficient series at shotpoint (SP) 16002. SP 16002 is the closest point of approach to Site 1224. The hydrothermal vein is identified with a reflection of reversed polarity relative to the seafloor reflection.

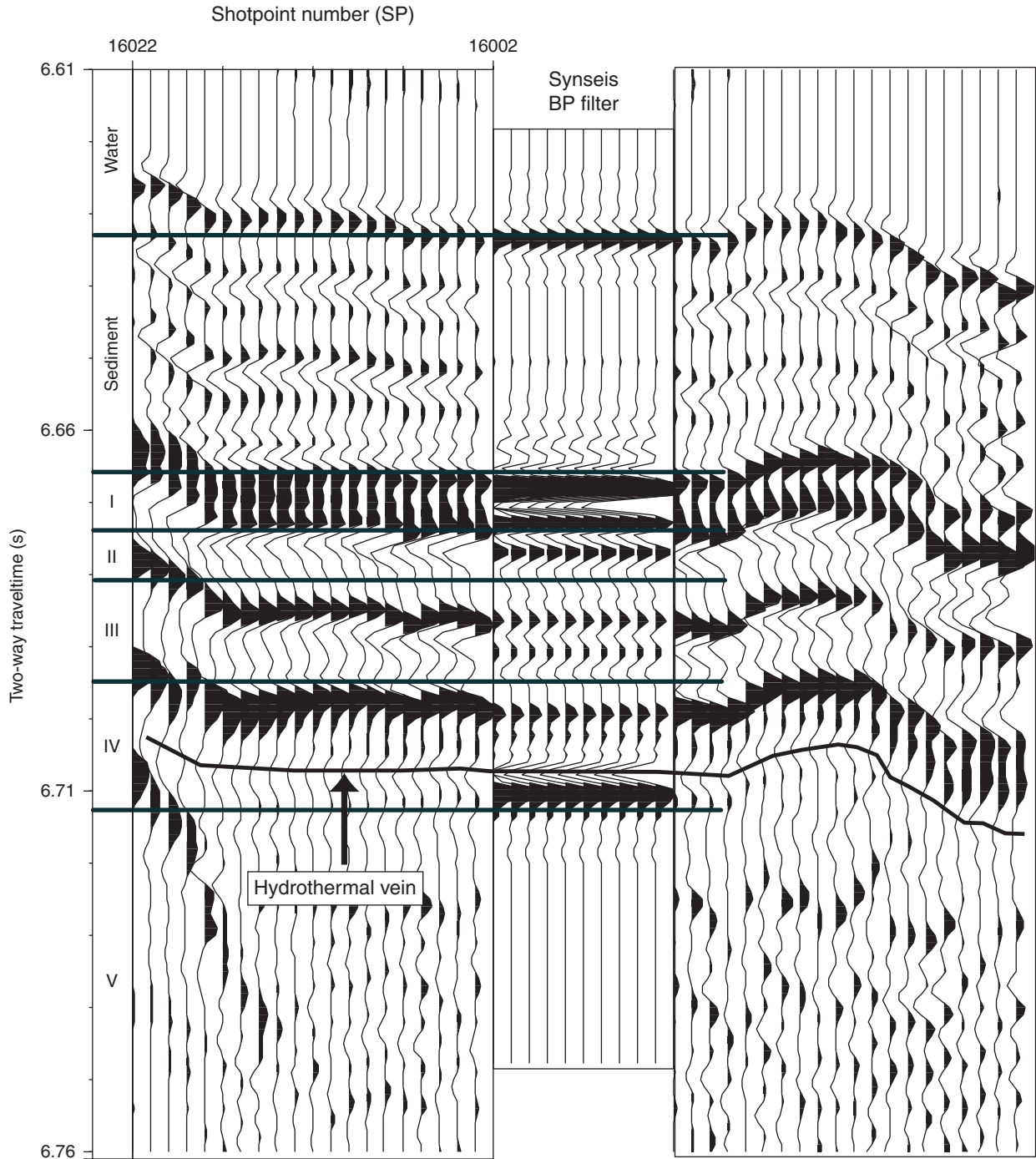


Figure F12. A portion of the SCS Line 14a at Site 1224 after bandpass filtering. Shotpoint (SP) 16002 is the closest point of approach to the site.

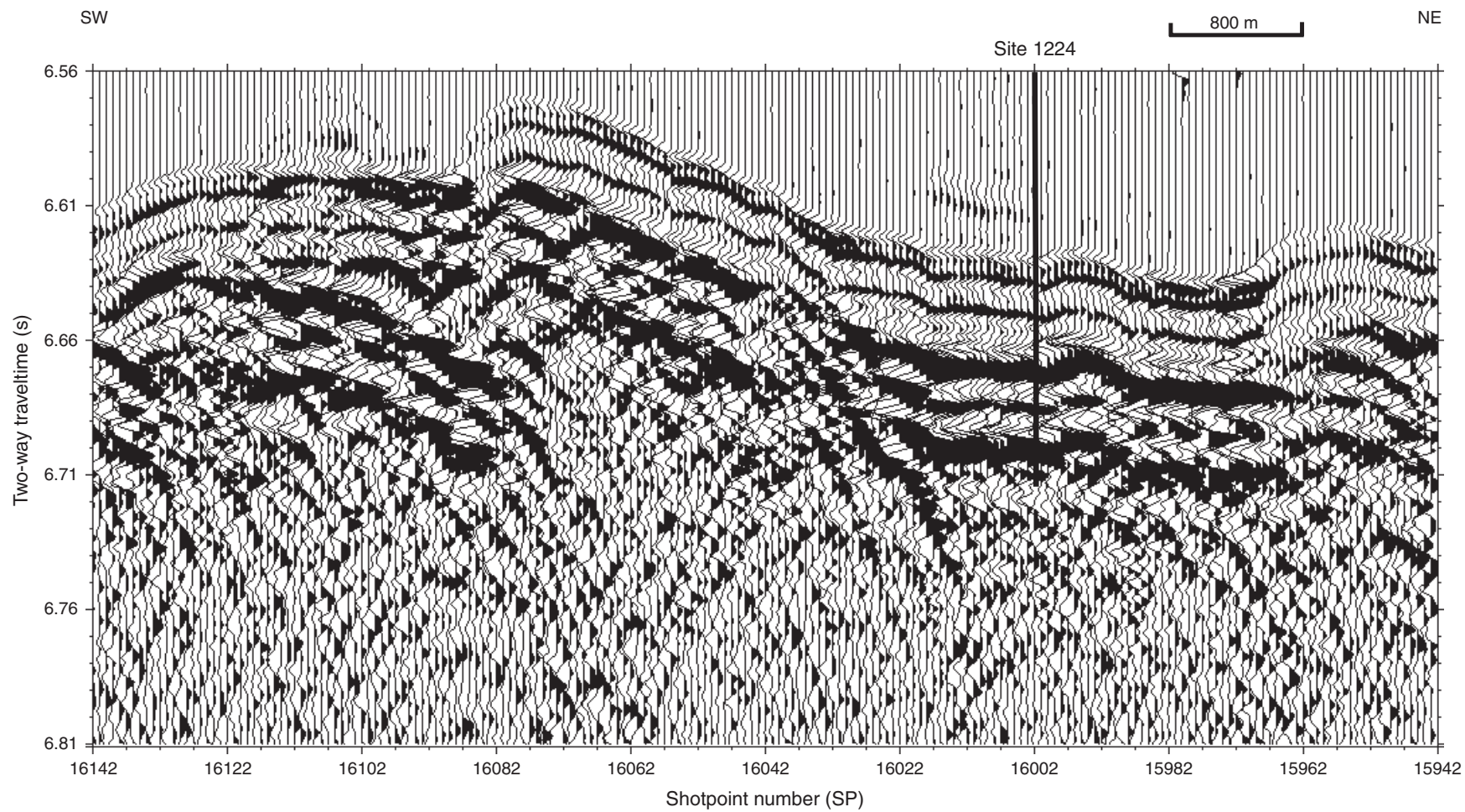


Figure F13. A portion of the SCS line around Site 1224 after seismic high-resolution processing. The five-layered basement structure of the oceanic crust is penetrated by Hole 1224F at this site, which is consistent with the logging-derived sequence units. Also shown is the hydrothermal vein connected to the seafloor by the fault at shotpoint (SP) 16040. SP 16002 is the closest point of approach to the site.

